TENSOR TOMOGRAPHY OF STRESS-INDUCED BIREFRINGENCE IN COMMERCIAL GLASSES

By

Carlos Andres Garavito-Garzon, Catherine A. Micek, Linh Viet Nguyen,
David C. Seal, Huan Sun, Evgeni Trofimov,
and
Douglas C. Allan

IMA Preprint Series # 2283

(October 2009)

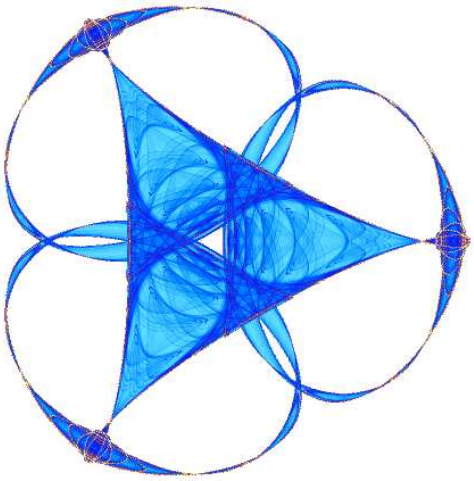

INSTITUTE FOR MATHEMATICS AND ITS APPLICATIONS

UNIVERSITY OF MINNESOTA
400 Lind Hall
207 Church Street S.E.
Minneapolis, Minnesota 55455–0436

Phone: 612/624-6066 Fax: 612/626-7370
URL: http://www.ima.umn.edu

Tensor Tomography of Stress-Induced Birefringence in Commercial Glasses

Carlos Andres Garavito-Garzon
Catherine A. Micek
Linh Viet Nguyen
David C. Seal
Huan Sun
Evgeni Trofimov
Mentor: Douglas C. Allan, Corning Incorporated

September 3, 2009

Abstract

This paper describes the progress and results of a 10-day Workshop on Mathematical Modeling in Industry XIII. Our team focused on the problem of understanding the stress state in a block of glass intended for use in making a photolithographic lens and relating those stresses to its birefringence. Our approach included studying both the "direct" problem, in which we derived a temperature distribution whose gradients approximates the stresses frozen into the glass during manufacturing, and the "inverse" problem, in which we seek to infer the internal stresses within the glass block based on measurements of birefringence along two axes. The latter is the "tensor tomography" problem mentioned in the title. Solution of the direct problem provided test data for studying the inverse problem. We chose to focus on an axisymmetric simplification since measured data show approximately axisymmetric optical properties. An important step toward explaining observed birefringence patterns was the solution of the steady-state temperature distribution in a cylindrical block of glass under slow cooling conditions. We exhibit that solution in this report and give details in an Appendix.

Contents

1 Introduction

1.1 Outline

This report is organized as follows: After an introduction and description of the problem, we elaborate first on the "direct" problem and second on the "inverse" problem, both described below. It will be shown that although we made very good progress on the direct problem, we only made limited progress on the inverse problem. Some comments are offered on possible difficulties in formulating the inverse problem. The main results obtained in our 10 days are described with a successful direct problem solution, where we show calculated temperature profiles, body forces, stresses, and, finally, predicted birefringence.

Birefringence refers to a different index of refraction for orthogonal light polarizations in a transparent material. In stress-free glasses (which are *isotropic* and can be made homogeneous), the birefringence is zero by symmetry. When such a glass is subjected to stress, even by squeezing between fingers, stress-induced birefringence is readily observed. In real glasses a certain amount of stress is unavoidably frozen in during glass annealing. The "fine annealing" of glass for optical applications is discussed in [1]. During the manufacture of pure silica glass (SiO_2) for photolithography lenses, the lens blank is heated above its annealing temperature and then cooled very slowly to minimize thermal gradients during cooling. Above the annealing temperature any stresses in the glass rapidly equilibrate through viscous flow of the glass, so stresses are zero even in the presence of thermal gradients. During cooling, it is impossible to completely prevent thermal gradients. This is because the temperature of the center, T_{center}, lags behind the temperature of the faces of the glass, T_{faces}, since the outside boundary temperatures are set by the furnace cooling rate. Slow cooling is used to minimize the thermal gradient (see Ref. [1]). A steady-state temperature profile is achieved during slow cooling when all transient thermal variations die away, and all points within the glass (and on its boundaries) continue to cool at the constant rate. The temperature profile during cooling is commonly approximated by the *thermal parabola*, which is a simple one-dimensional solution to the heat diffusion equation with a boundary condition of constant cooling rate. Once steady-state is achieved, the shape of the temperature profile becomes fixed (including of course its gradients) and *this temperature profile gives rise to the stresses frozen into the glass during*

annealing. Interestingly, the stress distribution in the glass after controlled cooling has the *opposite sign* to what would be expected purely on the basis of the thermal gradients. This arises because the steady-state temperature profile is achieved while the glass is still above its annealing temperature. In the presence of this thermal profile and the accompanying thermal strains, the glass is in a condition of zero stress. Upon cooling to room temperature, ultimately the center (hotter region during cooling) has to cool through a larger temperature change than the edges (cooler regions during cooling). Thus the center actually shrinks more relative to the faces and this extra shrinkage, taking place in a glass initially free from stress, produces tensile stress in the interior and compressive stress on the faces. This is the same phenomenon responsible for *thermal tempering*, or the strengthening of glass parts by introducing a compressive stress layer on the outside. The final stresses produced during cooling create strains in the glass that influence how the glass interacts with light, specifically producing stress-induced birefringence.

1.2 Description of Problem

The goal of our team was to develop mathematical models relating to stress-induced birefringence in Corning's lens blanks in order to provide insights that could lead to process improvements and better glass characterization. We sought to read limited sets of birefringence measurements and approximately reconstruct a stress distribution within the glass part that would be consistent with the measured birefringence scans, as well as develop tractable mathematical models which highlight selected sources of birefringence. An approximate reconstruction of stress is useful to understand what stresses exist in the sample, since knowledge about these stresses allows one to understand how the birefringence would be altered if glass were removed and the stress boundary conditions were changed. The project can be broken down into two pieces:

1. **The direct problem.** The "direct" problem consists of solving for stress in order to obtain birefringence. To accomplish this, we use finite element methods to solve the equilibrium equations of linear elasticity. The code we use is both "homegrown" Matlab code and commercial Ansys®code. Our own 3D Matlab code was written from scratch during the course of the workshop. An important component of this work is how to account for the pre-

existing stresses in the glass. This is accomplished by solving the steady-state heat equation on a cylindrical domain and using this as a body force in the calculations.

2. **The inverse problem.** The "inverse" problem consists of taking a given set of birefringence measures and re-constructing the stress from them. To accomplish this, we attempted to use an unconstrained, linear optimization algorithm implemented in Matlab.

Note that, although solving both of these problems is a large undertaking, it is useful because it allows us to check the accuracy of our work. On the direct problem, we made very good progress and gained useful new insights into the underlying problem. On the inverse problem, however, we made only limited progress because our several attempted approaches failed.

2 Direct Problem

In this section, we discuss results obtained from solving the direct problem. We first present a finite element method for pure traction boundary conditions on a general three-dimensional geometry. We then specialize the theory to our specific problem.

2.1 Finite Elements for Linear Elasticity

Let Ω denote the domain and denote its boundary as $\partial\Omega$. Let f be the prescribed body force per unit volume and s be an applied surface force. We recall that the *strong form* of the equilibrium equations for linear, isotropic elasticity with pure traction boundary conditions are

$$-\text{div } \sigma = f \text{ in } \Omega \tag{1}$$

$$\sigma \cdot n = s \text{ on } \partial\Omega \tag{2}$$

where σ is the linearized stress and n is an outward normal on the surface. The stress tensor σ is given in terms of the strain tensor ε, which is given in terms of gradients of displacements u :

$$\varepsilon_{ij} = \frac{1}{2}(u_{i,j} + u_{j,i}). \tag{3}$$

The comma indicates differentiation with respect to the indicated coordinate: explicitly, $u_{i,j} = \frac{\partial u_i}{\partial x_j}$. The stress is then related to the strain through Hooke's law:

$$\sigma_{ij} = 2\mu\varepsilon_{ij}(u) + \lambda\Delta\delta_{ij}, \tag{4}$$

where $\Delta = \text{trace}(\varepsilon)$ is the dilatation of the strain tensor and δ_{ij} is the identity tensor. Note the following:

- We have stresses from strains and strains from displacements, so displacements are the independent degrees of freedom in the problem.
- The parameters μ and λ are the Lamé constants. These are physical parameters that can be measured for a given material.

To use the finite element method, we must derive the *weak form* of the problem. Towards this end, we assert that finding a solution for the displacements u to the strong form of the boundary value problem is formally equivalent to finding a solution $u \in \mathbb{V}$ to the equation

$$a(u, v) = \ell(v), v \in \mathbb{V}, \tag{5}$$

where $\mathbb{V}$ is a Banach space, $a : \mathbb{V} \times \mathbb{V} \to \mathbb{R}$ is a bilinear form, and $\ell : \mathbb{V} \to \mathbb{R}$ is a linear functional.

Let our test function space be $\mathbb{V} = (H^1(\Omega))^n$ where $n = 3$ is the space dimension.[1] The weak form of the equilibrium equations can be obtained by multiplying the strong form by a test function $v \in \mathbb{V}$ and integrating by parts. Let $(\cdot, \cdot)$ denote the L^2 inner product. Explicitly:

$$\begin{aligned}(f, v)_\Omega = -(\text{div } \sigma, v)_\Omega &= -(\sigma n, v)_{\partial\Omega} + (\sigma, \nabla v)_\Omega \\ &= -(s, v)_{\partial\Omega} + (2\mu\varepsilon(u) + \lambda\varepsilon(u)I, \nabla v)_\Omega \\ &= -(s, v)_{\partial\Omega} + 2\mu(\varepsilon(u), \varepsilon(v))_\Omega + \lambda(\text{tr } \varepsilon(u), \text{tr } \varepsilon(v))_\Omega \\ &= -(s, v)_{\partial\Omega} + 2\mu(\varepsilon(u), \varepsilon(v))_\Omega + \lambda(\text{div } u, \text{div } v)_\Omega\end{aligned}$$

Notes on this derivation:

- The first line is the result of integration by parts.
- The traction boundary condition $\sigma \cdot n = s$ is enforced in the boundary integral.
- Our bilinear form $a(u, v) = 2\mu(\varepsilon(u), \varepsilon(v))_\Omega + \lambda(\text{div } u, \text{div } v)_\Omega$ and the linear form is $\ell(v) = (s, v)_{\partial\Omega} + (f, v)_\Omega$.
- Notice that the skew part of ∇v vanishes when multiplied by the symmetric strain tensor, $\varepsilon(u)$, and this leaves only the symmetric part of ∇v, $\varepsilon(v)$.

It is well-known from elasticity theory that boundary conditions such as Eq. 2 are not well-posed: the solution is non-unique because translations and rigid rotations are allowed. To avoid this issue while doing finite element analysis, it is necessary to fix various components of 3 nodes to have zero displacement. A more detailed discussion of this issue can be found in [2].

With the general theory now covered, we turn our attention to the specifics of our problem. We wrote a finite element code in Matlab

[1] The notation used here is the standard notation for Sobolev space $H^1(\Omega)$ and Lebesgue space $L^2(\Omega)$ in space dimension n:

$$H^1(\Omega) = \left\{ v \in L^2(\Omega) : \frac{\partial v}{\partial x_i} \in L^2(\Omega), i = 1, \ldots, n \right\}$$

where

$$L^2(\Omega) = \left\{ v : \Omega \to \mathbb{R} : \int_\Omega v^2 < \infty \right\}.$$

using the finite element formulation just described.[2] The domain was taken to be a 3-dimensional cylinder, i.e.

$$\Omega = \{0 < r < R, -L/2 < z < L/2, 0 < \theta < 2\pi\} \tag{6}$$

where R is the radius of the cylinder and L is the height of the cylinder. We enforce traction-free boundary conditions; specifically,

$$\sigma \cdot n = 0 \text{ on } \partial\Omega, \tag{7}$$

which is simply Eq. (2) with $s = 0$. The displacement components that we fix are as follows:

$$\begin{aligned} u_x(0,0,0) &= u_y(0,0,0) = u_z(0,0,0) = 0; \\ u_x(0,0,L/2) &= u_y(0,0,L/2) = 0; \\ u_x(R,0,0) &= 0, \end{aligned}$$

where u_i denotes the component of the displacement vector in the ith direction. Fixing the origin prevents rigid translations of the object. The last three components prevent rigid rotations over the remaining three degrees of freedom.

The body force f used in calculations represents the force given from the *residual stresses* present in the glass due to cooling. The analytical calculation of the body force is presented in Section 2.2. A numerical approximation of this solution is necessary and was implemented in Matlab, so it could be used in computations. In parallel with the effort to write a finite element code in Matlab, we also did FEM calculations using the commercial code Ansys®. The special features of Ansys allowed us to exploit the axisymmetric nature of the problem and simplify the complexity of the computations. The body force from residual stress was calculated by inputting temperatures on nodes and a thermal expansion coefficient so that Ansys could then calculate the corresponding body force. The use of Ansys allowed us to generate the results presented in later sections.

[2]This code was not brought to a useful working condition during this project. It was too slow even on a coarse grid.

2.2 Solution to Steady-State Cooling on Cylinder

2.2.1 The Heat Equation Model

In order to calculate residual stresses frozen in during cooling, a description of the steady-state temperature profile is needed. The gradient of this temperature profile produces the internal body forces, and this gives rise to the stresses in the material. The connection from temperatures to body forces is through strains and force balance; temperatures produce strains by thermal expansion, the strains are related to stresses through the stress-strain equations, and the negative of the divergence of the resulting stress tensor gives the body force from the temperature distribution. Thus body forces, which are a force per unit volume, are equivalent to the information contained in gradients of temperature. In our isotropic and linear elastic case the body forces are proportional to the gradient of temperature through factors of thermal expansion coefficient and Lamé constants in the form

$$F = -(3\lambda + 2\mu)\beta\nabla T \tag{8}$$

where λ and μ are Lamé constants and β is the coefficient of linear thermal expansion. A discussion of the relation between body forces and thermal gradients is given in Love [3]. In addition to the body force from thermal gradients, there is also a surface traction on $\partial\Omega$ given by

$$\sigma \cdot n = (3\lambda + 2\mu)\beta T \tag{9}$$

but this can be ignored because it only gives rise to a constant overall strain (and no stress) and therefore plays no role in our study of birefringence. Recall that the temperature on $\partial\Omega$ is a single value everywhere so this surface traction is merely an outward pressure on all points of the boundary of the sample. This would uniformly stretch (or shrink) the sample but would not create any stresses or any birefringence.

In order to minimize the gradient-induced forces during glass annealing, the glass part needs to cool at an extremely slow rate. The internal temperatures for silica glass being cooled at a *slow rate* for a long enough time (after temperature transients have died away) can

be modeled by the heat equation:

$$\begin{aligned} \kappa\nabla^2 T &= \frac{\partial T}{\partial t} \equiv \alpha \qquad \vec{x} \in \Omega \\ T &= T_0 + \alpha t \qquad \vec{x} \in \partial\Omega \end{aligned} \tag{10}$$

with $\alpha < 0$ a constant representing the slow cooling rate of the glass. The constant κ is called the thermal diffusivity constant which describes how easy it is for heat to diffuse in the material. The boundary conditions are defined by taking all points on the boundary of the block of glass to be fixed at the furnace temperature. That is, all points on the boundary are held at the same slowly diminishing temperature which is controlled by how the furnace is operated.

It may be of interest to solve for the steady-state temperature profile in an arbitrary geometry, but this is asking for too much. In order to make the problem more tractable and to address the geometry of greatest interest, we consider a perfect cylinder of height L and radius R. Our goal is to find the simplest possible solution that retains adequate complexity to represent useful insights into real glass samples and their birefringence. Since our geometry is simple, we are able produce an analytic solution. In the limit as the diameter of the cylinder approaches infinity, our solution duplicates the well known thermal parabola. The connection to the simpler one-dimensional problem is detailed in the Appendix.

2.2.2 Formal Solution

Consider the solid cylinder $\mathcal{C} := B(0,R) \times [-\frac{L}{2}, \frac{L}{2}]$, where $B(0,R)$ is the ball centered at the origin and $L > 0$. Let $T = T(\vec{x}, t)$ be a function defined on $\mathcal{C} \times [0, \infty)$. We call T a steady state temperature if it satisfies Equation (10) with $\Omega = \mathcal{C}$.

If we define the function U by

$$T(\vec{x}, t) = U(\vec{x}) + T_0 + \alpha t,$$

we can remove the time dependence of the heat equation. Solving our heat equation for T is now equivalent to solving for U, where U satisfies the boundary value elliptic problem

$$\begin{cases} \kappa\nabla^2 U(\vec{x}) = \alpha, & \vec{x} \in \mathcal{C} \\ U(\vec{x}) = 0, & \vec{x} \in \Gamma. \end{cases} \tag{11}$$

Here Γ is the boundary of $\mathcal{C}$, which is

$$\Gamma = S(0,R) \times \left[-\frac{L}{2}, \frac{L}{2}\right] \cup B(0,R) \times \left\{-\frac{L}{2}\right\} \cup B(0,R) \times \left\{\frac{L}{2}\right\}.$$

We only consider the axisymmetric solution U. U can be written as a series

$$U(r,z) = \sum_{m,n} A_{m,n} J_0\left(\frac{\gamma_m r}{R}\right) \cos\left(\frac{2\mu_n z}{L}\right), \quad m \geq 1, n \geq 0 \qquad (12)$$

where γ_m is the m^{th} zero of the Bessel function, $J_0(\gamma_m) = 0$, and $\mu_n = \pi(n + 1/2)$ is the $(n+1)^{\text{th}}$ zero of cosine, $\cos(\mu_n) = 0$. Using the orthogonality of the Bessel function and via direct calculation we have the following solution for the temperature profile:

$$A_{m,n} = \frac{\alpha}{\kappa} \frac{4(-1)^{n-1}}{\left[\left(\frac{\gamma_m}{R}\right)^2 + \left(\frac{2\mu_n}{L}\right)^2\right] J_1(\gamma_m)\gamma_m \mu_n}. \qquad (13)$$

A detailed derivation can be found in the appendix. Note that $A_{m,n}$ has units of temperature. The units of α (cooling rate) are degrees per second, κ is the thermal diffusivity which has units of length squared per time. Their ratio is degrees per length squared, but another factor of length squared arises from the R and L terms in the denominator so the result is a temperature in degrees.

Since we are only concerned with the gradient of the temperature, we need not concern ourselves with $T_0 + \alpha t$. That is, an overall change of temperature at all points in the sample will cause the entire sample to expand or contract, but, under the assumption of no clamping of the boundary, no stresses will result from this uniform dimensional change. Thus, $T_0 + \alpha t$ plays no role in the problem we consider.

A plot of the analytic solution is given in Figure [1]. The parabolic shape as a function of the sample height z, near the center of the sample, is obvious. A plot of the thermal gradients induced by this temperature distribution is given in Figures [2] and [3]. Note that the radial component of the body force is quite small until the radius approaches the cylinder boundary. This makes sense because near the radial center of the cylinder, there is no special direction along which a radial force would point, but as the boundary is approached it defines a direction or a perturbation that gives rise to a nonzero force. It will be seen below that this boundary effect also shows up in the stresses (and ultimately in the birefringence) near the boundary of the cylinder.

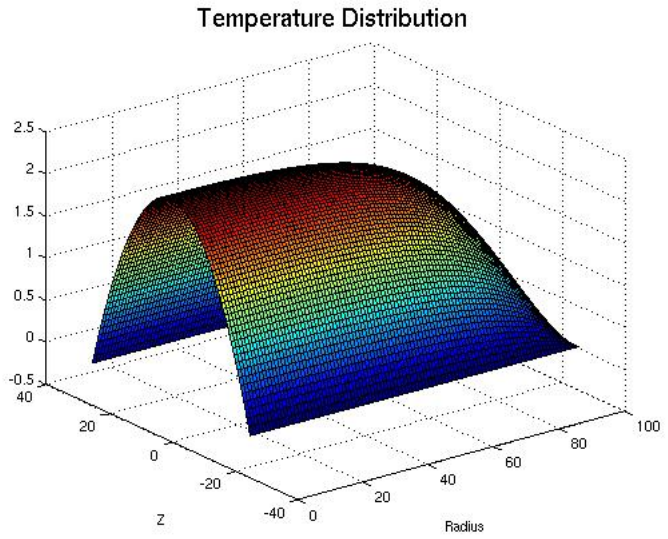

Figure 1: Temperature Distribution

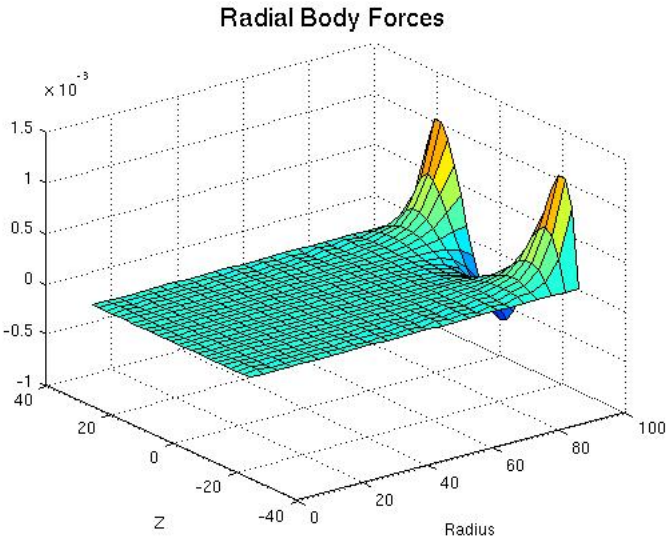

Figure 2: Radial Body Force

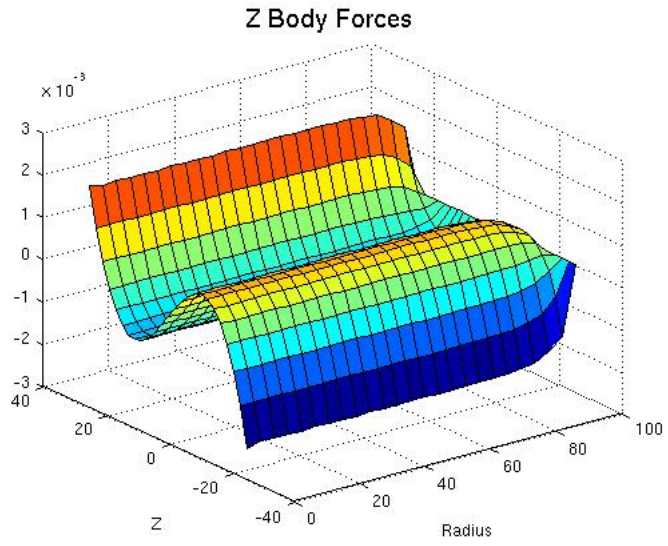

Figure 3: Z Body Force

2.3 Computing Birefringence

We use the body forces described above to calculate stresses by solving the equations for linear elasticity by finite element methods as described above. These stress components are then integrated along light paths downward (along z) and sideways (along r) and used in expressions given below to calculate predicted values for birefringence. The equations used in these calculations are described in the next section on the inverse problem.

One goal of these calculations was to create test data for the solving the inverse problem. A second goal was to examine the results in their own right and gain insight into the expected shapes of birefringence curves based on the exact cylinder steady-state cooling temperature profile. The results for averaged stress components and birefringence are given in Figures [4] and [5]. Features in both the top and side views in the birefringence correspond well with features seen in measured data (not shown). The magnitude of predicted birefringence values is in rough agreement with those of measured data, although a little lower, suggesting some adjustment of our thermal diffusivity or thermal expansion coefficient may be appropriate.

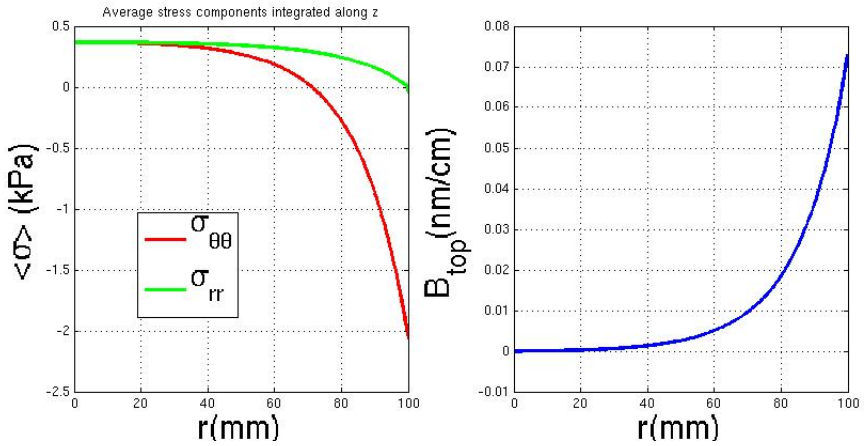

Figure 4: Averaged stress components and resulting birefringence viewed from top.

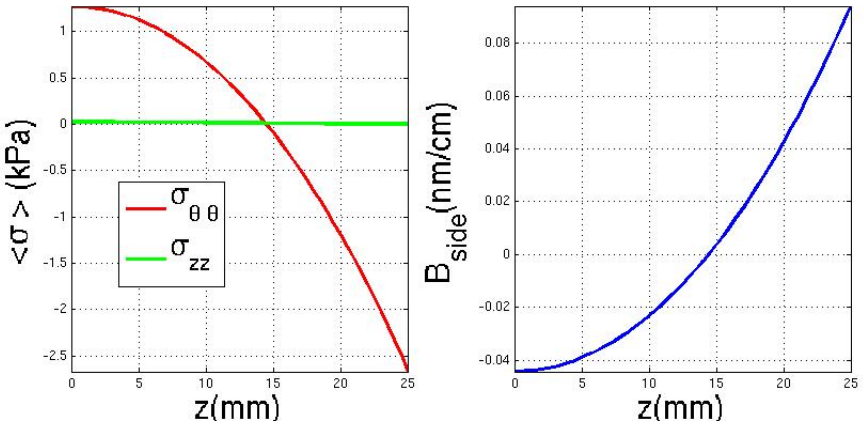

Figure 5: Averaged stress components and resulting birefringence viewed from side.

Strictly speaking, the thermal expansion is temperature-dependent, which we have ignored, and is larger than its room-temperature value when the temperature is raised. Our goal was to develop the simplest possible model capabable of reproducing the main features of measured data, so we have ignored such complexities. Both top and side views show a common theme: the main stress component is the tangential one $\sigma_{\theta\theta}$ in both cases. This makes sense from the following argument: as the glass cools, it is free to shrink both axially and radially, but it may not shrink "angularly". The only way to relieve the angular or tangential stress would be to remove a wedge of glass and reconnect the cylinder, like cutting out a piece of pie and then reforming the remaining pie into a smaller circle. Thus the two stress tensor components σ_{zz} and σ_{rr} do not contribute very much to the birefringence.

3 Inverse Problem

The inverse problem begins with measured birefringence values and attempts to compute physically feasible displacement-strain-stress values for points inside the studied object. With enough scans, one would theoretically be able to reproduce the exact displacement-strain-stress values. In our problem, we are restricted in the number of scans that are available to us because of a desire to minimize the cost of the measurements. Specifically, any light from a scan that does not go through the material perpendicular to the tangential plane experiences refraction. In order to avoid this phenomena one needs to use a "dunk tank" with index-matching oil which is a costly operation. For our problem, the information available to us are scans through the top and the side (through the central axis only in the side case) as indicated as in Figure [6]. Our group argues that the data available

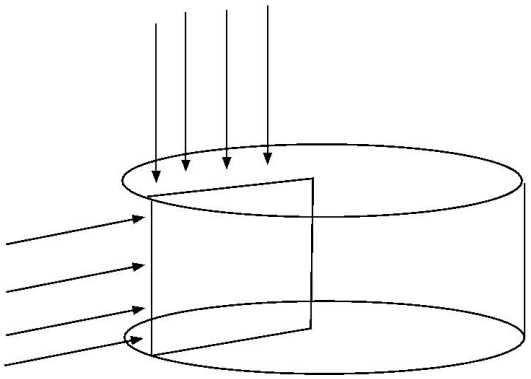

Figure 6: Measured Data

to us does not provide enough information to reproduce the desired quantities. Even assuming axisymmetry, given n scans from the side (through the z axis but sideways along r) and m scans from the top of the cylinder creates $2mn$ unknowns (two displacements per interior point) in the interior of the block. See Figure [7]. The unknowns are u_r and u_z, but the amount of information available to us scales like $3(m+n) \ll mn$. This argument makes clear that additional restrictions must be imposed on the allowed solutions in order to make the problem tractable. Part of those restrictions can come from physical considerations such as boundary conditions, force balance, and com-

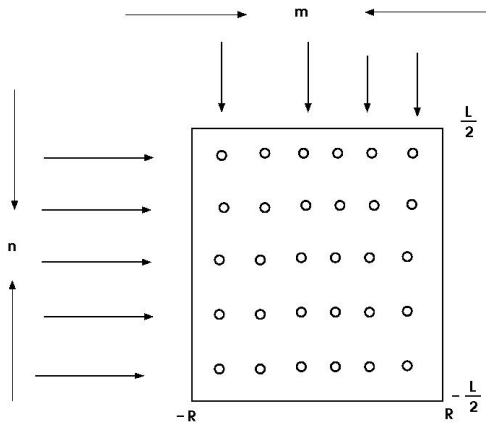

Figure 7: Number of measured data points

patibility relations, none of which are part of the raw birefringence data, but it appears that further restrictions are also required.

We were aware of the apparently ill-posed nature of the inverse problem but we hoped that by restricting the form of the solution to polynomial expansions of the displacements, as done in [6], that we might render the problem tractable. We did not complete a formal analysis of the well-posed-ness of the problem during our 10-day workshop, so this remains a topic of future investigation.

Recall the parameters R and L that describe the radius and length of the cylinder. We define the average values for the two available line scans as

$$\overline{\sigma}^{\mathrm{TOP}} = \frac{1}{L}\int_{z=-L/2}^{L/2} \sigma \; dz; \tag{14}$$

$$\overline{\sigma}^{\mathrm{SIDE}} = \frac{1}{R}\int_{r=0}^{R} \sigma \; dr. \tag{15}$$

The second integral has limits of integration $r = 0$ to $r = R$ even though the light is traveling through $r = -R$ to $r = R$. The contribution of the second half of the path is already included by symmetry and no additional factor is needed because we are calculating an average.

The assumption of axisymmetry simplifies the strain coefficients.

They are

$$\begin{aligned} \varepsilon_{rr} &= u_{r,r}, \qquad \varepsilon_{\theta\theta} = \frac{1}{r} u_r, \\ \varepsilon_{zz} &= u_{z,z}, \qquad \varepsilon_{rz} = \frac{1}{2} \left(u_{r,z} + u_{z,r} \right). \end{aligned} \tag{16}$$

The isotropic assumption yields

$$\begin{aligned} \sigma_{rr} &= \lambda\Delta + 2\mu\varepsilon_{rr}, \qquad \sigma_{\theta\theta} = \lambda\Delta + 2\mu\varepsilon_{\theta\theta} \\ \sigma_{zz} &= \lambda\Delta + 2\mu\varepsilon_{zz}, \qquad \sigma_{rz} = 2\mu\varepsilon_{rz}. \end{aligned} \tag{17}$$

with the dilatation defined as $\Delta = \varepsilon_{rr} + \varepsilon_{\theta\theta} + \varepsilon_{zz}$. The Appendix shows the equations relating strains to stresses in cylindrical coordinates in the general case, without the assumption of axisymmetry. Because of axisymmetry, one can derive the above relations by setting each $\frac{\partial}{\partial\theta} = 0$.

Using the relations between stress components and stress-induced birefringence,and assuming axisymmetry, we have

$$B^{\mathrm{TOP}} \cos(2\alpha_{\mathrm{slow}}) = C \left(\overline{\sigma}_{rr} - \overline{\sigma}_{\theta\theta} \right) \tag{18}$$

$$B^{\mathrm{SIDE}} \cos(2\alpha_{\mathrm{slow}}) = C \left(\overline{\sigma}_{zz} - \overline{\sigma}_{\theta\theta} \right). \tag{19}$$

C is the stress-optical constant, and we have measured values for a set of B^{TOP} and B^{SIDE} values and each α. Here α_{slow} is the "slow axis angle", or the angle of polarization that has the largest index of refraction. The birefringence for our axisymmetric problem is given by

$$B^{\mathrm{TOP}}(r) \cos(2\alpha) = \frac{2\mu C}{L} \int_{z=-L/2}^{L/2} \left(u_{r,r} - \frac{u_r}{r} \right) \, dz; \tag{20}$$

$$B^{\mathrm{SIDE}}(z) \cos(2\alpha) = \frac{2\mu C}{R} \int_{r=0}^{R} \left(u_{z,z} - \frac{u_r}{r} \right) \, dr \tag{21}$$

and the traction free boundary condition $\sigma \cdot n = 0$ can be stated as $\sigma_{rr}(R, z) = \sigma_{rz}(R, z) = 0$ and $\sigma_{zz}(r, \pm L/2) = \sigma_{rz}(r, \pm L/2) = 0$. Here and henceforth we will suppress the text *slow* in reference to the slow axis angle α_{slow}.

The data fitting technique we attempted was to expand the displacements u_r and u_z in terms of known functions. We chose to pursue polynomial expansions,although it may be more fruitful to use Chebychev polynomials or Bessel functions. In addition, it may be important

to try to incorporate physically realistic expansions into these models. For example, one would not want to use discontinuous expansions to describe a physically continuous medium.

The most simple fit we tried was

$$u_r = r\sum_{n\geq 0}(D_n r^n + F_n z^n), \tag{22}$$

$$u_z = \sum_{n\geq 0}(G_n r^n + K_n z^n), \tag{23}$$

with finitely many of the unknown constants D_n, F_n, G_n, K_n. We knew that we wanted $u_r = 0$ at $r = 0$ since there should be no radial displacement at the origin. A more general expansion could use a product of polynomials. This expansion takes the form

$$u_r = \left(\sum_{n\geq 1} a_n r^n\right)\left(\sum_{n\geq 0} b_n z^n\right); \tag{24}$$

$$u_z = \left(\sum_{n\geq 0} c_n r^n\right)\left(\sum_{n\geq 0} d_n z^n\right), \tag{25}$$

and again we insist that $u_r|_{r=0} = 0$ in order for our model to be physically consistent. If we use the simple sum of polynomials to fit the data, the expressions we obtain for measured birefringence are given by

$$B^{\mathrm{TOP}}(r)\cos(2\alpha) = 2\mu C\sum_{n\geq 0} nD_n r^n \quad \text{and} \tag{26}$$

$$B^{\mathrm{SIDE}}(z)\cos(2\alpha) = 2\mu C\sum_{n\geq 0}\frac{D_n}{n+1}R^n + F_n z^n - nK_n z^{n-1}.$$

The boundary condition constraints for the simple sum of polynomials

are given by

$$
\begin{aligned}
0 &= \sum_{n\geq 0}(n+1)D_n R^n + F_n z^n && (27)\\
0 &= \sum_{n\geq 0} nRF_n z^{n-1} + nG_n R^{n-1} && (28)\\
0 &= \sum_{n\geq 0} nK_n (L/2)^{n-1}(-1)^n && (29)\\
0 &= \sum_{n\geq 0} nF_n (L/2)^{n-1}(-1)^{n-1} + nG_n r^{n-1}. && (30)
\end{aligned}
$$

The first two equations come from enforcing the top boundary condition, the second two come from enforcing the bottom boundary condition.

If we use the more general product of polynomial expansion, we have measured birefringence values that are given by

$$
B^T(r)\cos(2\alpha) = 2\mu C \sum_{n\geq 2}(n-1)a_n r^{n-1} \cdot \sum_{\substack{n\,\geq\, 0\\ n \text{ is even}}} \frac{b_n}{n+1}\frac{L^n}{2^n}; \qquad (31)
$$

$$
\begin{aligned}
B^S(z)\cos(2\alpha) &= 2\mu C \left(\sum_{n\geq 1} n d_n z^{n-1} \cdot \sum_{n\geq 0} \frac{c_n}{n+1} R^n - \right. && (32)\\
&\qquad \left. \sum_{n\geq 0} b_n z^n \cdot \sum_{n\geq 1} \frac{a_n}{n} R^{n-1} \right).
\end{aligned}
$$

The coefficients a_n, b_n, c_n and d_n are unknowns of the problem. They can be found as solutions of the optimization problem and give minimum to the functional

$$
\begin{aligned}
F &= w_1 \sum_i \left(B^S(z_i) - B^S_{\text{meas}}(z_i)\right)^2\\
&\quad + w_2 \sum_i \left(B^T(r_i) - B^T_{\text{meas}}(r_i)\right)^2\\
&\quad + w_3 \sum_{i,j} (\text{BC Failure})_{i,j}
\end{aligned}
$$

Here the z_i, r_i are mesh points for variables z and r, B^S_{meas}, B^T_{meas} are experimentally measured and given data of birefringence, the last

term defines a boundary condition penalty that accounts for failure to exactly satisfy the boundary conditions, and w_1, w_2 and w_3 are weights. For the boundary conditions, σ_{rr}, σ_{zz} and σ_{rz} on the surfaces $r = R$ and $z = \pm L/2$, the equations are

$$\begin{aligned}(\text{BC Failure})_{i,j} &= \sigma_{rr}^2(R, z_j) + \sigma_{zz}^2(r_i, -L/2) + \sigma_{zz}^2(r_i, L/2) \\ &\quad + \sigma_{rz}^2(R, z_j) + \sigma_{rz}^2(r_i, -L/2) + \sigma_{rz}^2(r_i, L/2)\end{aligned}$$

where

$$\begin{aligned}\sigma_{rr} &= (\lambda + 2\mu) \sum_{n\geq 1} n a_n r^{n-1} \cdot \sum_{n\geq 0} b_n z^n + \frac{\lambda}{r} \sum_{n\geq 1} a_n r^n \cdot \sum_{n\geq 0} b_n z^n \\ &\quad + \lambda \sum_{n\geq 0} c_n r^n \cdot \sum_{n\geq 1} n d_n z^{n-1}, \\ \sigma_{zz} &= \lambda \sum_{n\geq 1} n a_n r^{n-1} \cdot \sum_{n\geq 0} b_n z^n + \frac{\lambda}{r} \sum_{n\geq 1} a_n r^n \cdot \sum_{n\geq 0} b_n z^n \\ &\quad + (\lambda + 2\mu) \sum_{n\geq 0} c_n r^n \cdot \sum_{n\geq 1} n d_n z^{n-1}, \\ \sigma_{rz} &= \mu \left(\sum_{n\geq 1} a_n r^n \cdot \sum_{n\geq 0} n b_n z^{n-1} + \sum_{n\geq 1} n c_n r^{n-1} \cdot \sum_{n\geq 0} d_n z^n \right),\end{aligned}$$

We used an internal Matlab implementation of the Levenberg-Marquardt algorithm in an attempt to solve this problem. Our results were unsatisfactory. The best fit solutions we discovered using this method were given by the zero function, and iterative convergence to this solution was obtained extremely fast. We believe the mathematical optimization problem may be ill-posed since we may not have a large enough data set to obtain a complete tomographic reconstruction. One item for future consideration might be to try to incorporate physically consistent constraints such as force balance into our ansatz. One major challenge our team encountered was a lack of experience with solving optimization problems. Our team treated the Matlab optimization software as a black box without fully understanding what type of problem formulation should provide satisfactory results.

4 Conclusion

When reading this manuscript it is important to remember that these results were generated in the course of a 10-day workshop that contained programmed interruptions, and that this work was performed by a team consisting of one mentor and six mathematics students with no previous exposure to this specific problem. In spite of this, a number of useful mathematical and physical insights were achieved. One significant achievement was the solution to the steady-state thermal profile for the cylinder geometry with constant cooling rate. This solution becomes the already familiar "cooling parabola" in the limit of large radius, as it must, but it provides a closer approximation to the real cooling-induced stresses taking appropriate boundary conditions into account at the radius of the cylinder. Using this temperature profile, we calculated the stress distribution that would be frozen into a cooling cylindrical block of glass and then we calculated the birefringence that would be observed from side and top. These results for birefringence resemble trends seen in measured data and offer insights into the physical causes of these observed measurements on the basis of how the samples are annealed. This information and similar information that can be gained by running additional calculations for other chosen geometries can help guide the understanding and suggest improved processing to minimize birefringence. In the other half of the project, the inverse problem, we have less concrete success. However, knowledge of what doesn't work is still extremely valuable since this provides focus for subsequent efforts to solve the inverse problem. Namely, our unsuccessful attempt at the tomographic reconstruction provides evidence that the problem as stated may not be well posed. As such, it may be necessary to perform additional birefringence scans to have enough information for an adequate reconstruction of internal stresses. The work provided in [6] indicates this is a concrete possibility. Considering that the primary goal of our project was to use mathematics to offer insight into the minimization of birefringence in high-quality optical glass, our project was successful.

References

[1] H.R. Lillie and H. N. Ritland, "Fine annealing of optical glass", *J. Amer. Cer. Soc.* Vol. 37[10], pages 466-473 (1954).

[2] M. Gockenbach, *Understanding and Implementing the Finite Element Method*, SIAM, 2006.

[3] A. E. H. Love, *A treatise on the mathematical theory of elasticity*, 4th edition, Dover, New York, 1944, page 108.

[4] G. B. Arfken, *Mathematical methods for physicists*, Orlando : Academic Press, c1985. Reprint of the second (1944) edition.

[5] Martin H. Sadd, *Elasticity Theory, Applications and Numerics*, Elsevier, 2009.

[6] J.F. Doyle and H.T. Danyluk, 1978 *Integrated Photoelasticity for Axisymmetric Problems*, Experimental Mechanics, Vol. 18, pages 215-220.

Appendix

A Steady-State Cooling

In this section we derive the solution U for (11). We assume that U is axisymmetric with respect to (x, y) and even with respect z. That is, $U = U(r, z)$ and $U(r, -z) = U(r, z)$ for $(r, z) \in [0, R] \times \left[-\frac{L}{2}, \frac{L}{2}\right]$. Equation (11) becomes

$$\left(\frac{1}{r}\frac{\partial}{\partial r} + \frac{\partial^2}{\partial r^2}\right) U(r, z) + \frac{\partial^2 U(r, z)}{\partial z^2} = \alpha, \tag{33}$$

with the zero boundary condition on Γ, which is redefined in terms of polar coordinates as follows

$$\Gamma := \{R\} \times \left[-\frac{L}{2}, \frac{L}{2}\right] \cup (0, R) \times \left\{\pm\frac{L}{2}\right\}.$$

Due to the boundary condition $U(r, z) = 0$ for $(r, z) \in \Gamma$, and assumption that U is even in z, we can write U in terms of series extension:

$$U(r, z) = \sum_{m\geq 1, n\geq 0} A_{m,n} J_0\left(\frac{\gamma_m r}{R}\right) \cos\left(\frac{2\mu_n z}{L}\right), \tag{34}$$

where γ_m is the m^{th} root of $J_0(\gamma)$, and $\mu_n = \pi\left(n + \frac{1}{2}\right)$ is the $(n+1)^{\text{th}}$ positive root of $\cos(\mu)$. It now suffices to compute $A_{m,n}$. One has

$$\begin{aligned}
\left(\frac{1}{r}\frac{\partial}{\partial r} + \frac{\partial^2}{\partial r^2}\right) J_0\left(\frac{\gamma_m r}{R}\right) &= -\left(\frac{\gamma_m}{R}\right)^2 J_0\left(\frac{\gamma_m r}{R}\right), \\
\frac{\partial^2}{\partial z^2}\left[\cos\left(\frac{2\mu_n z}{L}\right)\right] &= -\left(\frac{2\mu_n}{L}\right)^2 \cos\left(\frac{2\mu_n z}{L}\right).
\end{aligned}$$

Each term in our expansion will then have

$$\begin{aligned}
&\nabla^2\left[J_0\left(\frac{\gamma_m r}{R}\right)\cos\left(\frac{2\mu_n z}{L}\right)\right] = \\
&-\left[\left(\frac{\gamma_m}{R}\right)^2 + \left(\frac{2\mu_n}{L}\right)^2\right] J_0\left(\frac{\gamma_m r}{R}\right)\cos\left(\frac{2\mu_n z}{L}\right).
\end{aligned}$$

Substituting this result into our expansion (34), we arrive at

$$\nabla^2 U(r, z) = -\sum_{m,n} A_{m,n}\left[\left(\frac{\gamma_m}{R}\right)^2 + \left(\frac{2\mu_n}{L}\right)^2\right] J_0\left(\frac{\gamma_m r}{R}\right)\cos\left(\frac{2\mu_n z}{L}\right).$$

From equation (11), we obtain

$$-\frac{\alpha}{\kappa} = \sum_{m,n} A_{m,n} \left[\left(\frac{\gamma_m}{R}\right)^2 + \left(\frac{2\mu_n}{L}\right)^2 \right] J_0\left(\frac{\gamma_m r}{R}\right) \cos\left(\frac{2\mu_n z}{L}\right). \quad (35)$$

Let m', n' be any two natural numbers, multiplying both sides of the above equation with $rJ_0\left(\frac{\gamma_{m'} r}{R}\right)\cos\left(\frac{2\mu_{n'} z}{L}\right)$ and taking the integration on $\mathcal{C}$, we obtain

$$\sum_{m,n} A_{m,n} \left[\left(\frac{\gamma_m}{R}\right)^2 + \left(\frac{2\mu_n}{L}\right)^2 \right] a_{m,m'} b_{n,n'} = -\frac{\alpha}{\kappa} c_{m'} d_{n'}, \quad (36)$$

with each constant given by

$$\begin{aligned}
a_{m,m'} &= \int_0^R r J_0\left(\frac{\gamma_m r}{R}\right) J_0\left(\frac{\gamma_{m'} r}{R}\right) dr, \\
b_{n,n'} &= \int_{-\frac{L}{2}}^{\frac{L}{2}} \cos\left(\frac{2\mu_n z}{L}\right) \cos\left(\frac{2\mu_{n'} z}{L}\right) dz, \\
c_{m'} &= \int_0^R r J_0\left(\frac{\gamma_{m'} r}{R}\right) dr, \\
d_{n'} &= \int_{-\frac{L}{2}}^{\frac{L}{2}} \cos\left(\frac{2\mu_{n'} z}{L}\right) dz.
\end{aligned}$$

The orthogonality relationships of Bessel functions can be found in [4], and they provide a clean relationship for the above summand. They are

$$\begin{aligned}
a_{m,m'} &= \begin{cases} 0, \text{ if } m \neq m', \\ \frac{R^2}{2}[J_1(\gamma_m)]^2, \text{ if } m = m', \end{cases} \\
b_{n,n'} &= \begin{cases} 0, \text{ if } n \neq n', \\ \frac{L}{2}, \text{ if } n = n', \end{cases} \\
c_{m'} &= R^2 \frac{J_1(\gamma_{m'})}{\gamma_{m'}}, \\
d_{n'} &= \frac{(-1)^{n'} L}{\mu_{n'}}.
\end{aligned}$$

When we apply these results, we obtain

$$\begin{aligned} A_{m,n} &= -\frac{\alpha}{\kappa}\frac{c_m d_n}{\left[\left(\frac{\gamma_m}{R}\right)^2 + \left(\frac{2\mu_n}{L}\right)^2\right] a_{m,m} b_{n,n}} \\ &= \frac{\alpha}{\kappa}\frac{4(-1)^{n-1}}{\left[\left(\frac{\gamma_m}{R}\right)^2 + \left(\frac{2\mu_n}{L}\right)^2\right] J_1(\gamma_m)\gamma_m \mu_n} \end{aligned}$$

This completely solves our problem, since to compute $U(r,z)$, we need only compute γ_m and $J_1(\gamma_m)$, where γ_m are roots of J_0.

Another interesting quantity to compute is the temperature gradient $g = \nabla T$. With appropriate mechanical constants, the body force due to a temperature gradient can be related to the gradient g itself. To calculate the gradient from our temperature distribution, we have

$$\frac{\partial U}{\partial r} = -\sum_{m,n} \frac{\gamma_m}{R} A_{m,n} J_1\left(\frac{\gamma_m r}{R}\right) \cos\left(\frac{2\mu_n z}{L}\right), \tag{37}$$

$$\frac{\partial U}{\partial z} = -\sum_{m,n} \frac{2\mu_n}{L} A_{m,n} J_0\left(\frac{\gamma_m r}{R}\right) \sin\left(\frac{2\mu_n z}{L}\right). \tag{38}$$

In cylindrical coordinates, we have

$$\vec{g} = \frac{\partial U}{\partial r}\hat{r} + \frac{\partial U}{\partial z}\hat{z}.$$

The $\hat{\theta}$ component is 0 because the solution has no θ dependence due to the axisymmetry of the problem.

A.1 The one dimensional case

For a fixed $L > 0$, the temperature $T(x,y,z,t)$ found in the previous subsection depends on the radius R. We denote it by $T_R(x,y,z,t)$. We have $T(r,z,t) = U_R(r,z) + T_0 + \alpha t$, where

$$U_R(r,z) = \frac{4\alpha}{\kappa}\sum_{m=1}^{\infty}\sum_{n=0}^{\infty} \frac{(-1)^{n-1} J_0\left(\frac{\gamma_m r}{R}\right)\cos\left(\frac{2\mu_n z}{L}\right)}{\left[\left(\frac{\gamma_m}{R}\right)^2 + \left(\frac{2\mu_n}{L}\right)^2\right] J_1(\gamma_m)\gamma_m \mu_n}$$

Since $J_0(0) = 1$, we obtain

$$U_R(0,z) = \frac{4}{\pi\kappa}\sum_{m=1}^{\infty}\sum_{n=0}^{\infty} \frac{(-1)^{n-1}\cos\left(\frac{2\mu_n z}{L}\right)}{\left[\left(\frac{\gamma_m}{R}\right)^2 + \left(\frac{2\mu_n}{L}\right)^2\right] J_1(\gamma_m)\gamma_m \mu_n}.$$

We then observe that if $R \to \infty$, $U_R(0,z)$ converges to

$$V(z) = \frac{4\alpha}{\kappa} \sum_{m=1}^{\infty} \sum_{n=0}^{\infty} \frac{(-1)^{n-1} \cos\left(\frac{2\mu_n z}{L}\right)}{\left(\frac{2\mu_n}{L}\right)^2 J_1(\gamma_m)\gamma_m \mu_n}.$$

Recalling that $\mu_n = \pi\left(n + \frac{1}{2}\right)$, we obtain

$$V(z) = \frac{8\alpha L^2}{\pi^3 \kappa} \sum_{m=1}^{\infty} \frac{1}{J_1(\gamma_m)\gamma_m} \sum_{n=0}^{\infty} \frac{(-1)^{n-1} \cos\left(\frac{(2n+1)\pi z}{L}\right)}{(2n+1)^3}. \tag{39}$$

Running Matlab codes, we obtain

$$\sum_{m=1}^{\infty} \frac{1}{J_1(\gamma_m)\gamma_m} = \frac{1}{2}. \tag{40}$$

Lemma A.1. *Let*

$$g(z) := \frac{\pi^3}{8L^2}\left(z^2 - \frac{L^2}{4}\right).$$

Then for all $z \in \left[-\frac{L}{2}, \frac{L}{2}\right]$, *we have*

$$g(z) = \sum_{n=0}^{\infty} \frac{(-1)^{n-1} \cos\left(\frac{(2n+1)\pi z}{L}\right)}{(2n+1)^3}.$$

Proof Define a function h on $[-L, L]$ as follows

$$h(z) = \begin{cases} -h(z+L), & z \in \left[-L, -\frac{L}{2}\right], \\ h(z), & z \in \left[-\frac{L}{2}, \frac{L}{2}\right], \\ -h(L-z), & z \in \left[\frac{L}{2}, L\right]. \end{cases}$$

Consider the Fourier series extension of h on $[-L, L]$:

$$h(z) = d + \sum_{0}^{\infty} a_k \sin\left(\frac{k\pi}{L} z\right) + b_k \cos\left(\frac{k\pi}{L} z\right), \tag{41}$$

where

$$\begin{aligned} d &= \frac{1}{2L}\int_{-L}^{L} h(z)dz, \\ a_k &= \frac{1}{L}\int_{-L}^{L} h(z)\sin\left(\frac{k\pi}{L}z\right)dz, \\ b_k &= \frac{1}{L}\int_{-L}^{L} h(z)\cos\left(\frac{k\pi}{L}z\right)dz. \end{aligned}$$

Since h is an even function, we have $d = a_k = 0$. We now compute b_k:

$$\begin{aligned} b_k &= \frac{1}{L}\int_{-L}^{L} h(z)\cos\left(\frac{n\pi}{L}z\right)dz \\ &= \frac{2}{L}\int_{0}^{\frac{L}{2}} h(z)\left[\cos\left(\frac{k\pi}{L}z\right) - \cos\left(\frac{k\pi}{L}(L-z)\right)\right]dz \\ &= \frac{2}{L}\int_{0}^{\frac{L}{2}} h(z)\left[\cos\left(\frac{k\pi}{L}z\right) - (-1)^k\cos\left(\frac{k\pi}{L}z\right)\right]dz. \end{aligned}$$

Therefore $b_{2n} = 0$ and

$$\begin{aligned} b_{2n+1} &= \frac{4}{L}\int_{0}^{\frac{L}{2}} h(z)\cos\left(\frac{(2n+1)\pi}{L}z\right)dz \\ &= \frac{\pi^3}{2L^3}\int_{0}^{\frac{L}{2}}\left(z^2 - \frac{L^2}{4}\right)\cos\left(\frac{(2n+1)\pi}{L}z\right)dz, \\ &= \frac{\pi^3}{2L^3}\left[2(-1)^{n-1}\left(\frac{L}{(2n+1)\pi}\right)^3\right] \\ &= \frac{(-1)^{n-1}}{(2n+1)^3}. \end{aligned}$$

In summary, we arrive at

$$h(z) = \sum_{n=0}^{\infty} \frac{(-1)^{n-1} \cos\left(\frac{(2n+1)\pi z}{L}\right)}{(2n+1)^3},$$

for all $z \in [-L, L]$.

Since $g(z) = h(z)$ for all $z \in \left[-\frac{L}{2}, \frac{L}{2}\right]$, we conclude

$$g(z) = \sum_{n=0}^{\infty} \frac{(-1)^{n-1} \cos\left(\frac{(2n+1)\pi z}{L}\right)}{(2n+1)^3},$$

for all $z \in \left[-\frac{L}{2}, \frac{L}{2}\right]$.∎

Combining the above Lemma A.1, (40) and (39), we obtain

$$V(z) \quad = \quad \frac{\alpha}{2\kappa}\left(z^2 - \frac{L^2}{4}\right).$$

We observe that if we send $R \to \infty$, the finite cylinder $\mathcal{C}$ become the infinite slab

$$S = \left\{(x, y, z) : -\frac{L}{2} < z < \frac{L}{2}\right\},$$

whose boundary is

$$P_1 := \left\{(x, y, z) : z = -\frac{L}{2}\right\} \cup P_2 := \left\{(x, y, z) : z = \frac{L}{2}\right\}.$$

It is easy to check that $T(x, y, z, t) = V(z) + T_0 + \alpha t$ is the steady state on the infinite slab S:

$$\kappa \nabla^2 T(x, y, z, t) = \frac{\partial T(x, y, z, t)}{\partial t} = \alpha, \tag{42}$$

with the boundary condition

$$T(x, y, x, t) = T_0 + \alpha t.$$

In other words, we have shown that by sending $R \to \infty$, the steady-state temperature on the cylinder $\mathcal{C}$ approaches the one-dimensional steady state on the infinite slab S. Using the physical constants that describe silica being cooled at 1 degree C per hour, and with the sample geometry analyzed in the text with a radius of 100 mm and a length

of 50 mm, we find that the cylinder solution develops a temperature difference from center to edge that is about 0.988 of the temperature difference in the one-dimensional parabolic solution. Thus the z thermal gradients near the very center are about the same in the cylinder solution as in the one-dimensional parabolic solution. As seen in Figure [1], the cylinder solution begins to depart noticeably from the one-dimensional parabola solution about halfway to the radial edge.

B Equations of Elasticity in Different Coordinate Systems

The following set of relations can be found in Appendix A of Ref. [5]. The constants λ and μ are the Lamé constants and E and ν are the Young's modulus and the Poisson ratio. These are related by

$$\begin{aligned} \lambda &= \frac{E\nu}{(1+\nu)(1-2\nu)}, \\ \mu &= \frac{E}{2(1+\nu)}. \end{aligned} \tag{43}$$

B.1 Strain Displacement Relations

B.1.1 Cartesian Coordinates

$$\begin{aligned} \varepsilon_{xx} &= \frac{\partial u_x}{\partial x}, \\ \varepsilon_{yy} &= \frac{\partial u_y}{\partial y}, \\ \varepsilon_{zz} &= \frac{\partial u_z}{\partial z}, \\ \varepsilon_{xy} &= \frac{1}{2}\left(\frac{\partial u_x}{\partial y} + \frac{\partial u_y}{\partial x}\right), \\ \varepsilon_{xy} &= \frac{1}{2}\left(\frac{\partial u_y}{\partial z} + \frac{\partial u_z}{\partial y}\right), \\ \varepsilon_{xy} &= \frac{1}{2}\left(\frac{\partial u_z}{\partial x} + \frac{\partial u_x}{\partial z}\right). \end{aligned} \tag{44}$$

B.1.2 Cylindrical Coordinates

$$
\begin{aligned}
\varepsilon_{rr} &= \frac{\partial u_r}{\partial r}, \\
\varepsilon_{\theta\theta} &= \frac{1}{r}\left(u_r + \frac{\partial u_\theta}{\partial \theta}\right), \\
\varepsilon_{zz} &= \frac{\partial u_z}{\partial z}, \\
\varepsilon_{r\theta} &= \frac{1}{2}\left(\frac{1}{r}\frac{\partial u_r}{\partial \theta} + \frac{\partial u_\theta}{\partial r} - \frac{u_\theta}{r}\right), \\
\varepsilon_{\theta z} &= \frac{1}{2}\left(\frac{\partial u_\theta}{\partial z} + \frac{1}{r}\frac{\partial u_z}{\partial \theta}\right), \\
\varepsilon_{rz} &= \frac{1}{2}\left(\frac{\partial u_r}{\partial z} + \frac{\partial u_z}{\partial r}\right).
\end{aligned} \tag{45}
$$

B.2 Equilibrium Equation

B.2.1 Cartesian Coordinates

$$
\begin{aligned}
\frac{\partial \sigma_{xx}}{\partial x} + \frac{\partial \sigma_{yx}}{\partial y} + \frac{\partial \sigma_{zx}}{\partial z} + f_x &= 0, \\
\frac{\partial \sigma_{xy}}{\partial x} + \frac{\partial \sigma_{yy}}{\partial y} + \frac{\partial \sigma_{zy}}{\partial z} + f_y &= 0, \\
\frac{\partial \sigma_{xz}}{\partial x} + \frac{\partial \sigma_{yz}}{\partial y} + \frac{\partial \sigma_{zz}}{\partial z} + f_z &= 0.
\end{aligned} \tag{46}
$$

B.2.2 Cylindrical Coordinates

$$
\begin{aligned}
\frac{\partial \sigma_{rr}}{\partial r} + \frac{1}{r}\frac{\partial \sigma_{r\theta}}{\partial \theta} + \frac{\partial \sigma_{rz}}{\partial z} + \frac{1}{r}(\sigma_{rr} - \sigma_{\theta\theta}) + f_r &= 0, \\
\frac{\partial \sigma_{r\theta}}{\partial r} + \frac{1}{r}\frac{\partial \sigma_{\theta\theta}}{\partial \theta} + \frac{\partial \sigma_{\theta z}}{\partial z} + \frac{2}{r}\sigma_{r\theta} + f_\theta &= 0, \\
\frac{\partial \sigma_{rz}}{\partial r} + \frac{1}{r}\frac{\partial \sigma_{\theta z}}{\partial \theta} + \frac{\partial \sigma_{zz}}{\partial z} + \frac{1}{r}\sigma_{rz} + f_z &= 0.
\end{aligned} \tag{47}
$$

B.3 Hooke's Law

The relation between stress and strain in Hooke's law is similar in Cartesian and cylindrical coordinate systems, as follows:

B.3.1 Cartesian Coordinates

$$\begin{aligned}
\sigma_{xx} &= \lambda(\varepsilon_{xx}+\varepsilon_{yy}+\varepsilon_{zz})+2\mu\varepsilon_{xx}, \qquad \varepsilon_{xx} = \frac{1}{E}[\sigma_{xx}-\nu(\sigma_{yy}+\sigma_{zz})], \quad (48)\\
\sigma_{yy} &= \lambda(\varepsilon_{xx}+\varepsilon_{yy}+\varepsilon_{zz})+2\mu\varepsilon_{yy}, \qquad \varepsilon_{yy} = \frac{1}{E}[\sigma_{yy}-\nu(\sigma_{zz}+\sigma_{xx})],\\
\sigma_{zz} &= \lambda(\varepsilon_{xx}+\varepsilon_{yy}+\varepsilon_{zz})+2\mu\varepsilon_{zz}, \qquad \varepsilon_{zz} = \frac{1}{E}[\sigma_{zz}-\nu(\sigma_{xx}+\sigma_{yy})],\\
\sigma_{xy} &= 2\mu\varepsilon_{xy}, \qquad \varepsilon_{xy} = \frac{1+\nu}{E}\sigma_{xy},\\
\sigma_{yz} &= 2\mu\varepsilon_{yz}, \qquad \varepsilon_{yz} = \frac{1+\nu}{E}\sigma_{yz},\\
\sigma_{zx} &= 2\mu\varepsilon_{zx}, \qquad \varepsilon_{zx} = \frac{1+\nu}{E}\sigma_{zx}.
\end{aligned}$$

B.3.2 Cylindrical Coordinates

$$\begin{aligned}
\sigma_{rr} &= \lambda(\varepsilon_{rr}+\varepsilon_{\theta\theta}+\varepsilon_{zz})+2\mu\varepsilon_{rr}, \qquad \varepsilon_{rr} = \frac{1}{E}[\sigma_{rr}-\nu(\sigma_{\theta\theta}+\sigma_{zz})], \quad (49)\\
\sigma_{\theta\theta} &= \lambda(\varepsilon_{rr}+\varepsilon_{\theta\theta}+\varepsilon_{zz})+2\mu\varepsilon_{\theta\theta}, \qquad \varepsilon_{\theta\theta} = \frac{1}{E}[\sigma_{\theta\theta}-\nu(\sigma_{zz}+\sigma_{rr})],\\
\sigma_{zz} &= \lambda(\varepsilon_{rr}+\varepsilon_{\theta\theta}+\varepsilon_{zz})+2\mu\varepsilon_{zz}, \qquad \varepsilon_{zz} = \frac{1}{E}[\sigma_{zz}-\nu(\sigma_{rr}+\sigma_{\theta\theta})],\\
\sigma_{r\theta} &= 2\mu\varepsilon_{r\theta}, \qquad \varepsilon_{r\theta} = \frac{1+\nu}{E}\sigma_{r\theta},\\
\sigma_{\theta z} &= 2\mu\varepsilon_{\theta z}, \qquad \varepsilon_{\theta z} = \frac{1+\nu}{E}\sigma_{\theta z},\\
\sigma_{zr} &= 2\mu\varepsilon_{zr}, \qquad \varepsilon_{zr} = \frac{1+\nu}{E}\sigma_{zr}.
\end{aligned}$$